THE ASTROPHYSICAL JOURNAL, 219:727–739, 1978 January 15

RADIAL DEPENDENCE OF SOLAR WIND PROPERTIES DEDUCED FROM *HELIOS 1/2* AND *PIONEER 10/11* RADIO SCATTERING OBSERVATIONS

RICHARD WOO
Jet Propulsion Laboratory, California Institute of Technology
Received 1977 May 12; accepted 1977 July 22

ABSTRACT

In this paper we present the results of radio scattering measurements conducted at 2.3 GHz over an extensive heliocentric distance range (1.7–180 $R_\odot$) of the solar wind using the *Helios 1/2* and *Pioneer 10/11* spacecraft. Spectral broadening has been observed closer to the Sun than ever before, and, when combined with the first measurement of angular broadening of a spacecraft signal, yields a solar wind velocity of 24 km s^{-1} at 1.7 $R_\odot$, a result that is estimated to be accurate to within a factor of 2–2.5. By assuming that the rms density fluctuation σ_{ne} is proportional to the mean density n_e, and using Saito's density model, we have obtained the velocity profile of the acceleration region of the solar wind. The results are consistent with the few existing velocity measurements made by other radio techniques as well as some existing theoretical models of the solar wind. Phase or Doppler scintillations, which are shown to be proportional to $\sigma_{ne}v^{5/6}$ (v is the solar wind velocity), have been measured out to 180 $R_\odot$. Beyond 10 $R_\odot$ the radial dependence of the phase scintillations is roughly $R^{-1.3}$, and, within the assumptions that $\sigma_{ne} \propto n_e$ and $v^{5/6} \sim v$, suggest that the solar wind is slightly converging in the equatorial region between approximately 20 and 180 $R_\odot$.

Subject headings: radio sources: general — Sun: solar wind

I. INTRODUCTION

Radio observations during the solar occultations of natural sources as well as spacecraft signals represent an important tool for studying the radial dependence of solar wind parameters because they can be conducted over a wide range of heliocentric distances including regions that have not yet been probed by direct spacecraft or studied by photometric means. Angular broadening (Erickson 1964; Slee 1966; Okoye and Hewish 1967; Vitkevich and Vlasov 1972; Blesing and Dennison 1972; Ward 1975) and intensity scintillations (Hewish and Symonds 1969; Cohen and Gunderman 1969; Watanabe, Shibasaki, and Kakinuma 1972; Rao, Bhandari, and Ananthakrishnan 1974; Coles, Rickett, and Rumsey 1974) represent two scattering phenomena that have been widely used to study the variation of electron density fluctuations and solar wind velocity with heliocentric distance. Additional scattering phenomena which are now possible with coherent and monochromatic spacecraft signals include spectral broadening (Goldstein 1969; Woo, Yang, and Ishimaru 1976, hereafter referred to as Paper I) and phase scintillations (Woo *et al.* 1976). Unlike intensity scintillations and angular broadening which measure electron density fluctuations, spectral broadening measures a combination of electron density fluctuations and solar wind velocity (Paper I), and, as we will show in this paper, so do phase scintillations. The purpose of this paper is to present and discuss extensive radio scattering measurements made with the *Helios 1/2* and *Pioneer 10/11* spacecraft.

II. SPECTRAL AND ANGULAR BROADENING

The *Helios 1/2* spacecraft were launched into orbital trajectories around the Sun on 1974 December 10 and 1976 January 15, respectively. Since then these spacecraft have performed a multitude of important direct measurements of the interplanetary medium in the heliocentric distance range of 0.3–1.0 AU.

Figures 1 and 2 are the fixed Earth-Sun line trajectories for *Helios 1* in 1975 and *Helios 2* in 1976, respectively. The plane of the figures represents the ecliptic and the celestial north pole is above it. For *Helios 1* there were two periods in 1975 when extensive spectral broadening observations were conducted: the first one (April 13–June 8) when the ray path reached a minimum heliocentric distance of 1.6 $R_\odot$ on the west side of the Sun, the second one (August 27–September 3) when the spacecraft completely disappeared behind the Sun. Although there were three solar occultations of *Helios 2* in 1976, data were obtained only during the first (May 7–24) and third (September 18–20). The second occultation was not tracked because it coincided with the *Viking* Mars landings.

Three features of the *Helios* trajectories make the radio measurements invaluable. First, because the ray paths are in the ecliptic plane, the observations are essentially of the equatorial region and latitudinal effects need not be considered. Second, since these measurements occurred during the solar cycle minimum, solar transient events such as those seen by *Pioneer 6* during the solar cycle maximum (Goldstein

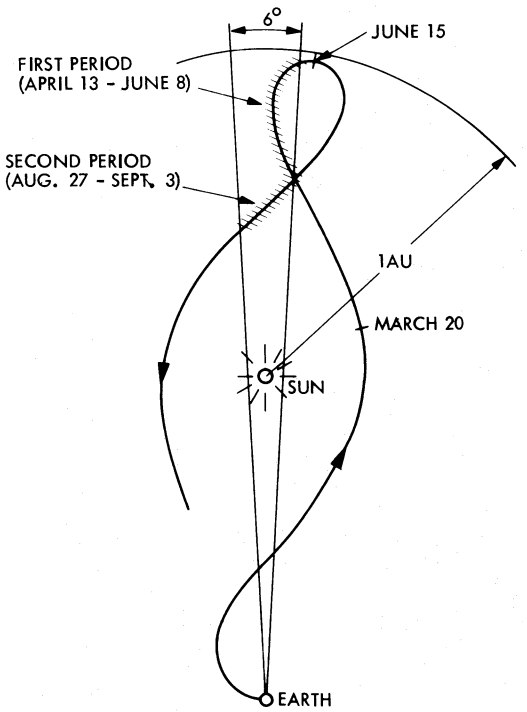

FIG. 1.—Fixed Earth-Sun line trajectory for *Helios 1* in 1975. The plane of the figure is the ecliptic, and the celestial north pole is above it.

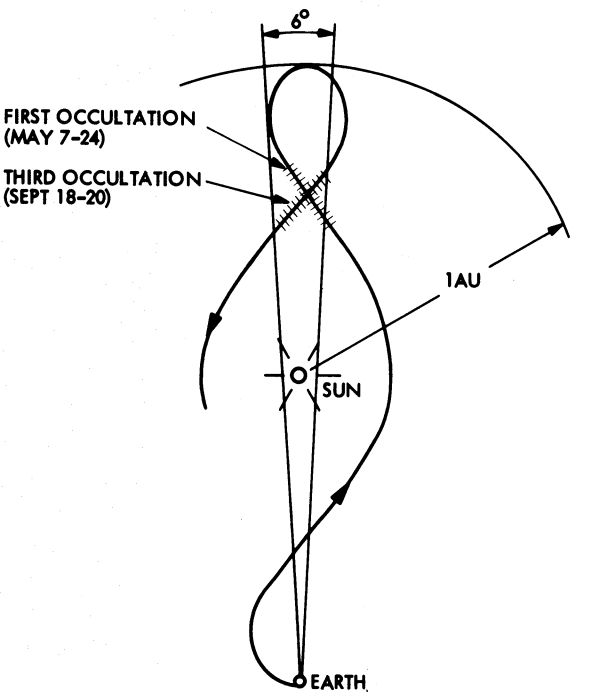

FIG. 2.—Fixed Earth-Sun line trajectory for *Helios 2* in 1976. Similar to Fig. 1.

1969) are minimized; in fact, none were observed during the *Helios* spectral broadening experiments. As a result, the *Helios* measurements are ideal for studying the "background" turbulence. Finally, during the first period of *Helios 1* (April 13–June 8), the radio signal probed within 12 $R_\odot$ for approximately two solar rotations, thus providing an important opportunity to separate the spatial and temporal variations.

The *Helios* spacecraft operated in two radio transmission modes. In the one-way mode, the 2.3 GHz (13 cm) spacecraft signal, which is linearly polarized, is transmitted to the ground receiver, the signal traversing the corona once. In the two-way mode, the signal is transmitted from Earth to the spacecraft and back to Earth, the signal traversing the corona twice. It is obvious that for probing the solar corona, one-way measurements are preferred since the interpretation of two-way data requires knowledge of the performance of the spacecraft transponder under noisy conditions. Even though both types of data were collected, we will present and discuss only the one-way data in this paper.

The experimental system used to make the spectral broadening measurements is similar to that described by Goldstein (1969). The received radio signal was maintained within the passband of the open-loop or wide-band receiver by a local oscillator which was programmed to remove the large Doppler shifts in frequency due to the relative motion of the spacecraft and receiver. The frequency band which was observed was varied between 100 and 500 Hz. The primary data are the power spectrograms of the S-band carrier. The signals were sampled digitally and converted into power spectra by the discrete Fourier transform. Each group of 1024 samples of the signal waveform was transformed to produce 512 points on the spectrum; this resulted in a frequency resolution ranging from $\sim$0.2 Hz for the 100 Hz bandwidth to $\sim$1.0 Hz for the 500 Hz bandwidth. Averaged data were displayed on an *x-y* plotter in real time and stored on magnetic tape for further processing. System tests have shown that the stability of the combination of transmitter, programmed local oscillator, and spectrum analyzer is generally better than 0.2 Hz over a time scale of 20 min.

The 64 m antenna located at NASA's Goldstone Tracking Station was used for receiving the S-band signal. The antenna receiver system is extremely sensitive and has an equivalent noise temperature of about 19 K. At this noise temperature, the signal-to-noise ratio (SNR) in a 1 Hz bandwidth for the *Helios* signal is about 40 dB and represents an improvement of approximately 16 dB over *Pioneer 6*. This fact along with the relatively quiet Sun conditions resulted in measurements of spectral broadening made closer to the Sun than ever before ($\sim$1.7 $R_\odot$).

Data were taken almost daily during the periods indicated in Figures 1 and 2. The actual schedule each day was variable, depending on conflicting demands for the 64 m antenna, but generally an hour of data was obtained each day. All of the data were collected in the form of spectrograms, with each

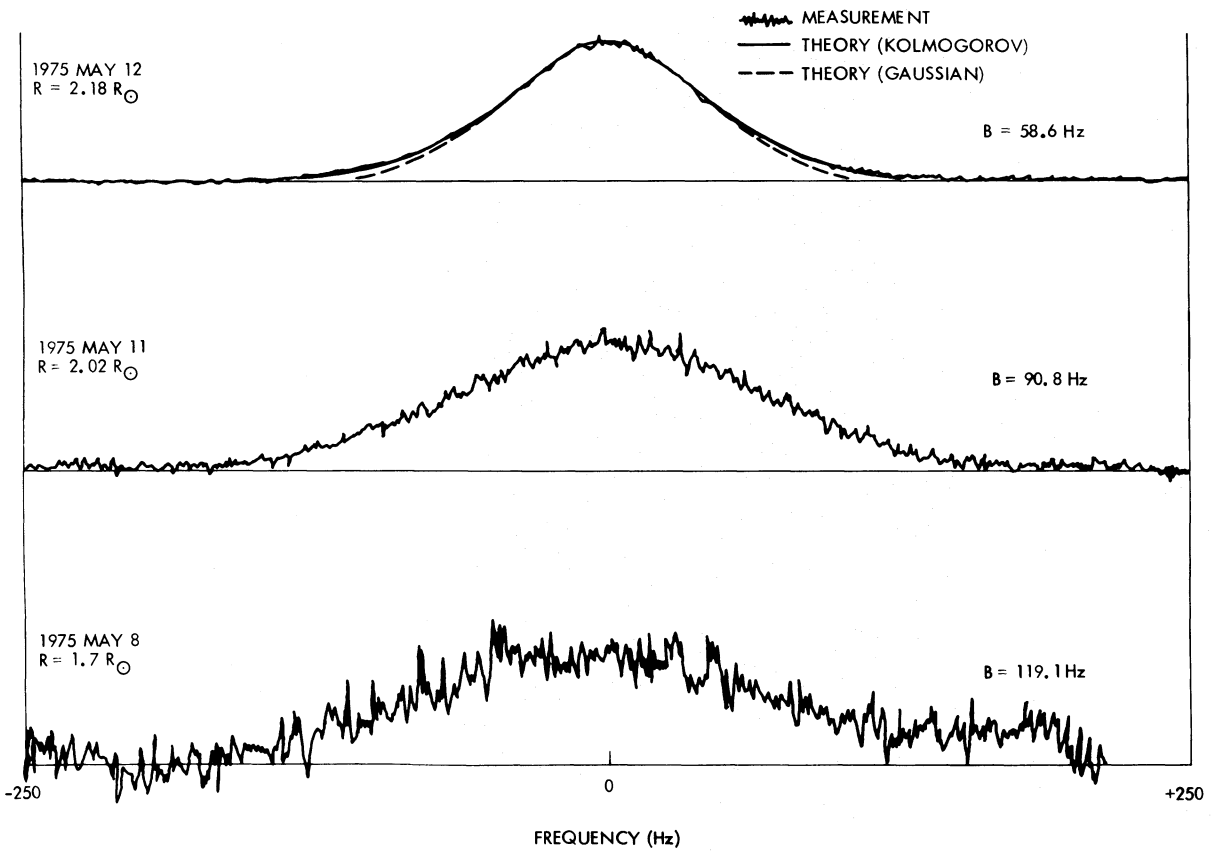

FIG. 3.—Helios spectrograms

spectrogram the result of 20 minutes of observation.

Three spectrograms which were measured close to the Sun are shown in Figure 3. The bandwidth for each is 500 Hz. The spectrogram at the top was obtained on 1975 May 12 when the closest approach distance was 2.18 $R_\odot$. Despite the close proximity to the Sun, it is remarkably smooth, a direct consequence of the excellent SNR. Superposed on the measured May 12 spectrogram is the theoretical curve corresponding to the case where the spectrum of the electron density fluctuations is power law with a spectral index of 11/3 (Kolmogorov spectrum). As in previous studies (Paper I), the agreement between theory and experiment is excellent; in fact, the measured and theoretical curves are almost indistinguishable. For the sake of comparison, we have fitted the measured spectrogram with a Gaussian curve (corresponding to a Gaussian density spectrum) by matching it at half-maximum. While the agreement is equally good for the lower frequencies, it is not as good at the high-frequency end. The determination of the spectral index from the shape of the spectrogram is even more meaningful now that we know that the shape of the spectrogram is not affected by the anisotropy of the electron density fluctuations or the velocity fluctuations in the solar wind (Woo, Yang, and Ishimaru 1977, hereafter referred to as Paper II).

Each spectrogram was processed to determine the bandwidth B defined in the following way:

$$\int_0^{B/2} P(f)df = \tfrac{1}{2}\int_0^{\infty} P(f)df, \qquad (1)$$

where $P(f)$ is the spectrogram of the received signal. The variation of B with heliocentric distance is shown in Figure 4. The scatter in the data, which represents changes in the solar corona rather than measurement error, amounts to a factor of about 2. As mentioned earlier, no solar transient events of the type seen by *Pioneer 6* during the solar maximum were observed during the solar minimum *Helios* measurements, so that the data in Figure 4 are excellent for studying and interpreting the radial dependence of spectral broadening.

The measurement closest to the Sun was obtained on 1975 May 8 when the closest approach distance R was 1.7 $R_\odot$ and the system temperature had risen to 850 K; the respective spectrogram is shown in Figure 3. It is clear that between 2.18 $R_\odot$ and 1.7 $R_\odot$ the signal undergoes a rapid deterioration in SNR. By comparing the integrated spectrograms and the system noise temperatures on May 8 with those corresponding to May 23 when R was 5.02 $R_\odot$, it was found that there was a loss in SNR of 4.52 dB over and above

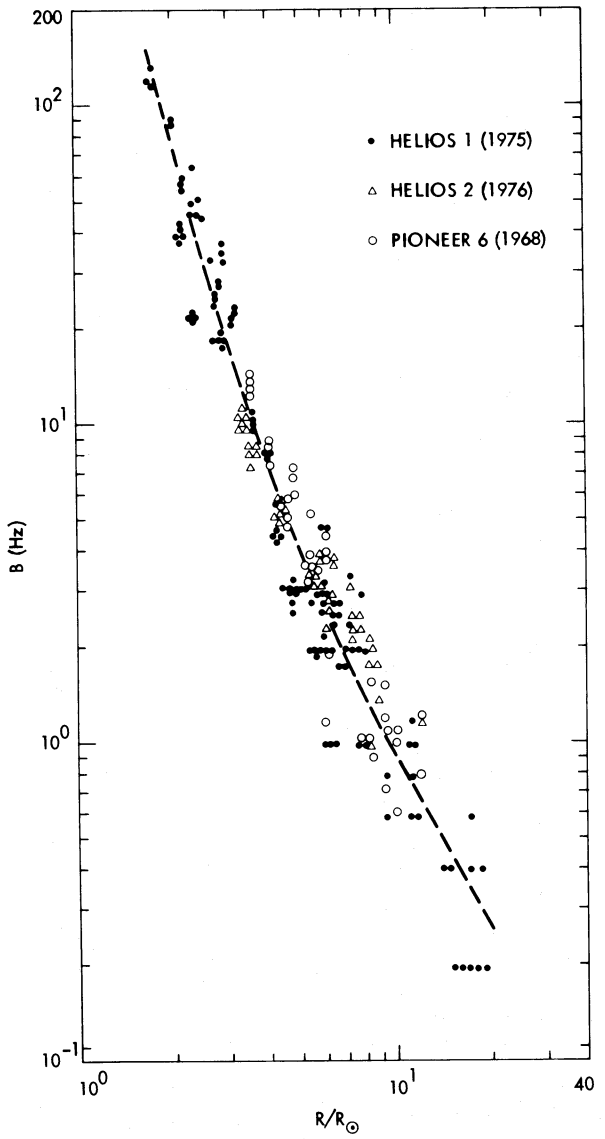

FIG. 4.—Radial dependence of spectral broadening. The dashed line represents an approximation to the data.

that due to the increase in temperature. The apparent reason for this loss is that the *Helios* point source was broadened by the electron density fluctuations to the extent that it was larger than the beamwidth of the receiving antenna. The fact that an angular broadening effect was observed at the same time as spectral broadening is invaluable because it is possible to deduce a measurement of solar wind velocity from such combined measurements (Paper II).

Let us estimate the loss in power due to angular broadening. The 64 m antenna pattern is circularly symmetric, and we will approximate it by a Gaussian function with a beamwidth θ_{BW}, the angular half-width to e^{-1}. Comparison of the Gaussian function with the actual antenna pattern shows that it is an excellent choice and that at S-band, $\theta_{BW} = 0.^\circ08475$ (Bathker 1973). The angular spectrum of a point source broadened by turbulence is also well approximated by a Gaussian function, and the contour of equal intensity is an ellipse whose axial ratio we will define as being Q (Paper II; Blesing and Dennison 1972; Dennison and Blesing 1972). We will define the beamwidth θ_{AB} to be the angular half-width to e^{-1} along the minor axis of the ellipse. Then, the ratio of signal power in the presence of angular broadening to that when there is no broadening P_{RATIO} is given by

$$P_{RATIO} = \left\{\left[1 + \left(\frac{\theta_{AB}}{\theta_{BW}}\right)^2\right]\left[1 + \left(Q\,\frac{\theta_{AB}}{\theta_{BW}}\right)^2\right]\right\}^{-1/2}. \quad (2)$$

As would be expected, when $\theta_{AB} = 0$, $P_{RATIO} = 1$. Also, when $Q = 1$ (circularly symmetric angular spectrum) and $\theta_{AB} = \theta_{BW}$, $P_{RATIO} = 0.5$. Computed results of P_{RATIO} as a function of θ_{AB}/θ_{BW} for various values of Q are shown in Figure 5. Equation (2) can be written alternately as

$$\frac{\theta_{AB}}{\theta_{BW}} = \left[\left[\frac{1}{2}\left\{-\left(1 + \frac{1}{Q^2}\right) + \left[\left(1 + \frac{1}{Q^2}\right) - 4\left(\frac{1}{Q^2} - \frac{1}{P^2Q^2}\right)\right]^{1/2}\right\}\right]^{1/2}, \quad (3)$$

where $P = P_{RATIO}$.

Near the Sun the effects of refraction may be as important as angular broadening (Hewish 1968). If we use the electron densities given by Saito (1970) and the results derived by Kliore, Cain, and Hamilton (1964) for bending angle and defocusing attenuation (due to differential refraction), we find that at 1.7 $R_\odot$ the angle of refraction ϵ is 0.'8 and that the attenuation due to defocusing is 0.296 dB. Since the plasma collision frequency is much less than the radio frequency even at 1.7 $R_\odot$, the absorption by the solar corona is negligible. The loss in SNR between 5.02 $R_\odot$ and 1.7 $R_\odot$ attributable to angular broadening is, therefore, 4.52–0.296 = 4.22 dB so that $P = 0.378$. Two-dimensional brightness distribution observations conducted near the solar cycle minimum in 1973 and 1974 (Ward 1975) indicate that in the heliocentric distance range of 5–15 $R_\odot$ the axial ratio Q is always less than 2 and that it exhibits little or no dependence on heliocentric distance. It is likely that this situation persists in 1975 even as close in as 1.7 $R_\odot$, and for this reason we will assume that $Q = 2$. Using the result that $P = 0.378$, we find from equation (3) that $\theta_{AB}/\theta_{BW} = 0.867$, and since $\theta_{BW} = 0.^\circ08475$, $\theta_{AB} = 4.'41$ (full width of 8.'82). Along the major axis of the ellipse the half-width angle to e^{-1} is 8.'82 (full width 17.'63). Thus, at 1.7 $R_\odot$ the effect of refraction at S-band is negligible when compared to the extent of angular broadening.

The *Helios* angular broadening measurement at 1.7 $R_\odot$ represents the first angular broadening measurement of a spacecraft signal, and it would be interesting to compare it with similar observations of natural

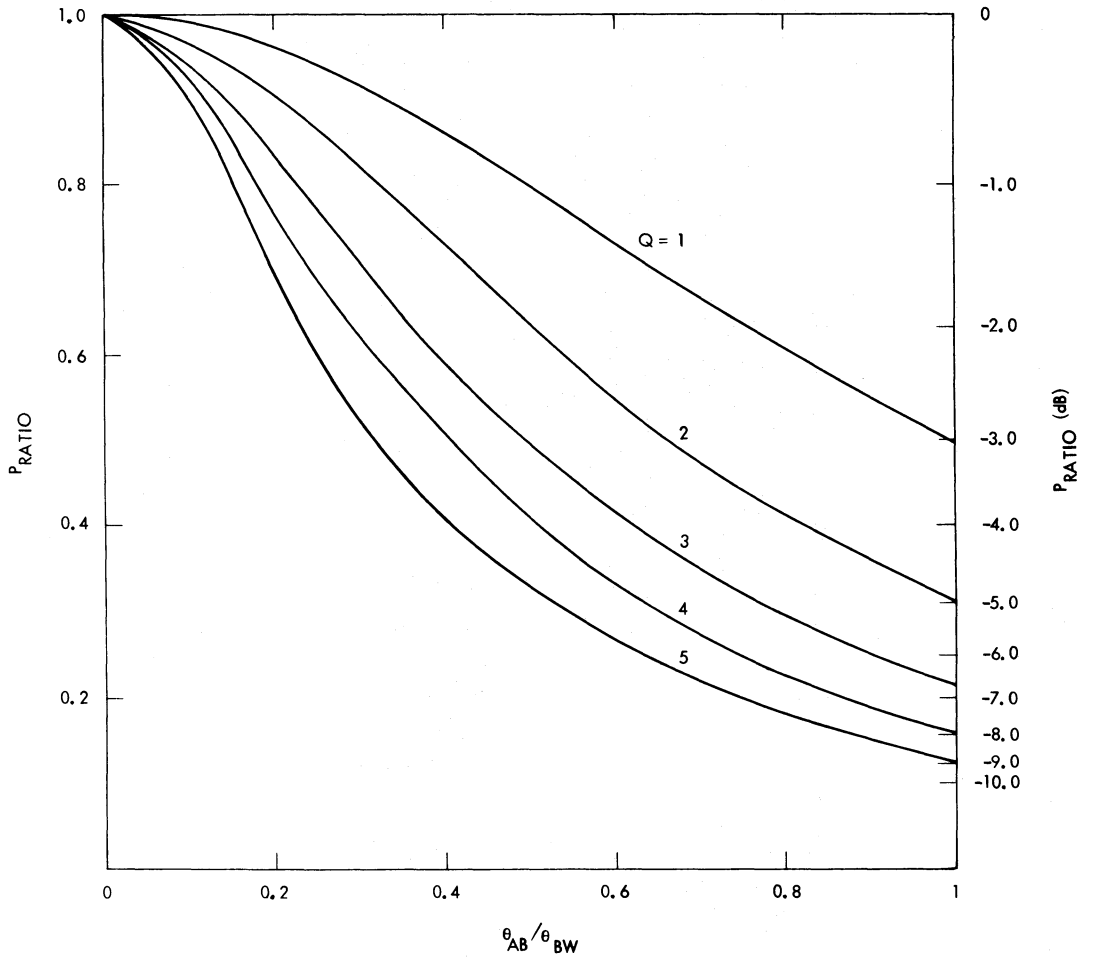

FIG. 5.—Computed results for P_{RATIO}, the ratio of signal power in the presence of angular broadening to that when there is no broadening.

radio sources. To convert the *Helios* spherical-wave measurement to an equivalent plane-wave measurement, we multiply the former by the factor L_2/L (Paper II) and obtain 4.03 for the semimajor axis. We have scaled Ward's (1975) summary of the variation of the tangential scattering to 2.3 GHz according to k^{-2}, and plotted the results along with the plane-wave converted *Helios* measurement in Figure 6. Data prior to 1968 are from Okoye and Hewish (1964), the 1969–1971 data from Blesing and Dennison (1972), and the 1973–1974 data from Ward (1975). As can be seen, the *Helios* result is consistent with the natural radio source observations farther out. In comparing the 1975 *Helios* measurement at 1.7 $R_\odot$ with that of the 1974 Crab Nebula at 5 $R_\odot$, we find, as might be expected from previous studies (Erickson 1964), that the scattering is very nearly proportional to the mean density as given by Newkirk (1967) and Saito (1970). In fact, that the density fluctuations are proportional to the mean density is an assumption that will be made later in this paper. It should be noted that the radial dependence would be steeper if a $k^{-2.2}$ dependence (corresponding to the Kolmogorov spectrum) were assumed (Paper II).

Let us deduce the solar wind velocity at 1.7 $R_\odot$ from the angular and spectral broadening measurements. The relevant geometries are shown in Figure 7. From Paper II the solar wind velocity $v = |v|$ is given by

$$v = 5.77 \frac{B}{\theta} \frac{L}{kL_2} \left(\sin^2 \phi + \frac{\cos^2 \phi}{Q^2} \right)^{-1/2} \times (\sin^2 \gamma + Q^2 \cos^2 \gamma)^{-1/2}, \quad (4)$$

where θ is the angular half-width to e^{-1} measured in the plane which makes an angle γ with $\boldsymbol{B}$, the projection of the magnetic field on the plane transverse to the ray path (see Fig. 7*a*), k is the wavenumber, ϕ is the angle the velocity makes with $\boldsymbol{B}$, $L = L_1 + L_2$, and L_1 and L_2 are the distances defined in Figure 7*b*. Note that for $\gamma = 0$, $\theta = \theta_{AB}$. We will assume that the solar wind is parallel to the magnetic field so that $\phi = 0$. This seems reasonable since the wind is radially

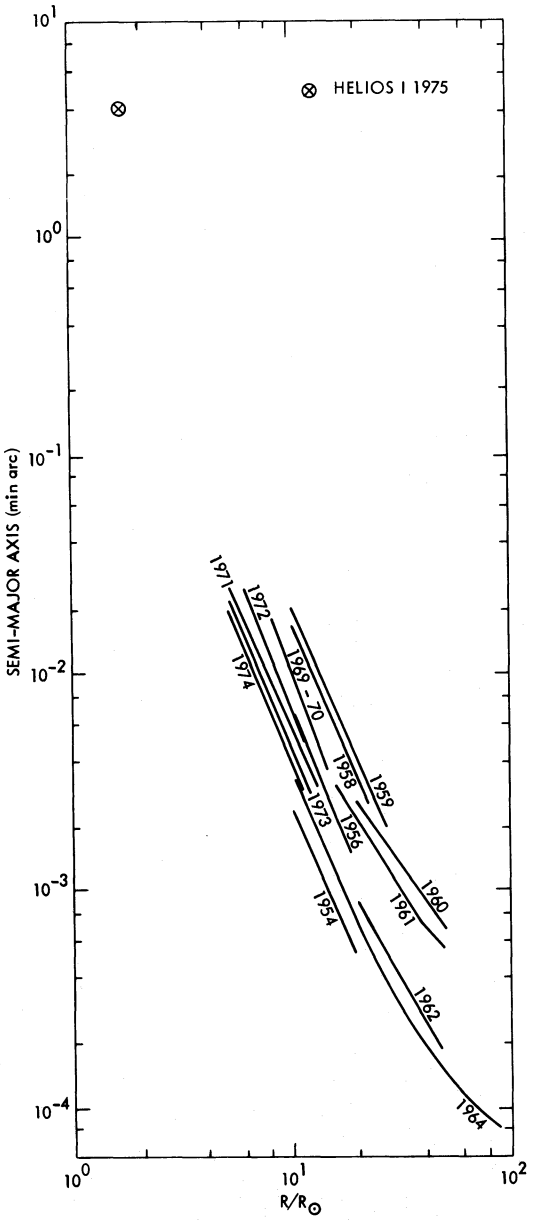

FIG. 6.—Variation of tangential scattering (semimajor axis) as a function of distance from the Sun at 2.3 GHz. Except for the *Helios* measurement at 1.7 $R_\odot$, all measurements were conducted at lower frequencies using natural radio sources and were scaled to 2.3 GHz according to a k^{-2} dependence. The lower-frequency data were taken from a summary by Ward (1975); data prior to 1968 were from Okoye and Hewish (1967), the 1969–1971 data from Blesing and Dennison (1972), and the 1973–1974 data from Ward (1975).

directed and the magnetic field is also, even at distances as close as 1.7 $R_\odot$ when the Sun is quiet (Waldmeier 1977). The angular broadening data (Ward 1975) show that the magnetic field is indeed radial in the heliocentric distance range of 5–15 $R_\odot$. The measured bandwidth B at 1.7 $R_\odot$ was 119.1 Hz. From the trajectory of *Helios 1*, $L_1 = 1.0$ AU and $L_2 = 0.84$ AU; and substituting these results into equation (4), we find that the solar wind velocity v at 1.7 $R_\odot$ is 24 km s^{-1}.

Let us examine the uncertainty in this velocity measurement. The least known information used in deducing this result is that concerning the axial ratio Q which we assumed to be 2. Near the Sun it is quite possible that Q could be larger. The two-dimensional brightness distribution observations (Blesing and Dennison 1972) show that at least during the higher portion of the solar cycle the axial ratio shows a tendency to increase to 4–5 near 5 $R_\odot$. From Figure 5, we note that for $P = 0.378$, increasing Q from 2 to 5 decreases θ_{AB}/θ_{BW} by a factor of 2; and since velocity is inversely proportional to θ_{AB}, this has the effect of doubling the velocity estimate. Thus, if Q is between 2 and 5 rather than equal to 2, the velocity estimate is low by at most a factor of 2. Another assumption made was that the solar wind is parallel to the magnetic field $\boldsymbol{B}$ so that $\phi = 0$. At distances as close as 1.7 $R_\odot$ it is certainly possible that the magnetic field lines are closed and that $\phi \neq 0$. Under these circumstances, it can be seen from equation (4) that the velocity may be decreased by as much as a factor of Q. Thus, when $Q = 5$ and if $\phi = 0$, the velocity estimate of 24 km s^{-1} must be increased by a factor of 2; and if $\phi \neq 0$, the estimate can be decreased by as much as a factor of 5/2 = 2.5. Two other factors affect the accuracy of the velocity measurement. First of all, there is the effect of velocity fluctuation. Ekers and Little (1971) have shown that the velocity fluctuations near 1.7 $R_\odot$ may be twice as high as the mean velocity. From Paper II we see that when $\sigma_v/v = 2$, where σ_v is the rms velocity fluctuation, the bandwidth B is reduced by 30%, which leads to an underestimate of velocity by the same factor. The other effect is that of velocity projection (Jokipii and Lee 1972, 1973), which is very small at 1.7 $R_\odot$ because of the steep radial dependence of the structure constant c_n. In view of the above discussion, we feel that the velocity estimate of 24 km s^{-1} is probably good to within a factor of 2–2.5. The method for measuring velocity just described is best employed during the lower portion of the solar cycle, when it appears from the angular broadening results that the axial ratio and, therefore, the measurement uncertainty is most likely to be minimized. Of course, such uncertainties are eliminated if complete two-dimensional brightness distribution observations are available at the same time.

For the sake of comparison we have included in Figure 4 the *Pioneer 6* measurements of the background turbulence (Paper I) which are also of the equatorial region. It is interesting to note that despite the disparity in time with respect to the solar cycle, the *Pioneer 6* measurements appear to be within the scatter of the *Helios* data. Of course, measurements corresponding to "solar events" (as defined in Goldstein 1969) have been removed from the *Pioneer 6* data (Paper I), and this would tend to make the data set low. It is clear that additional observations, particularly during the solar cycle maximum, need to be

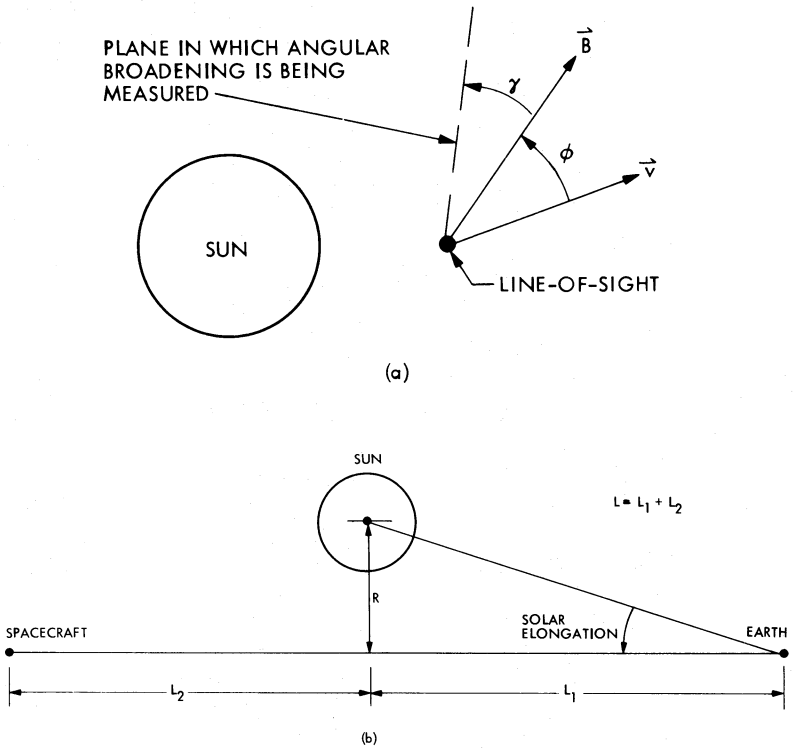

FIG. 7.—Geometry of solar occultation observations. (*a*) View of Sun from Earth; (*b*) line-of-sight path

conducted before firm conclusions can be drawn about the solar cycle dependence. Although an increase in turbulence increases the bandwidth, an increase in the axial ratio which appears to accompany the increase in turbulence (Ward 1975) decreases it (Paper II). Still, angular broadening is affected in a similar way (Paper II) and observations of this phenomenon show a definite correlation with the solar cycle (Okoye and Hewish 1967; Blesing and Dennison 1972; Ward 1975). Of course, all this means is that the effect of the increased turbulence exceeds that due to the increased anisotropy. One point of difference that may also be important is the fact that the angular broadening observations contain the effects of "solar events" whereas the *Pioneer 6* results do not.

Drawn in Figure 4 is a dashed line representing an approximation of the radial dependence of the spectral broadening data. The approximation in the 10–20 $R_\odot$ region is based on both spectral broadening and Doppler scintillations which will be discussed in § III. Let us derive the solar wind profile from this result. We assume that the rms electron density fluctuation σ_{ne} is proportional to electron density n_e, a result that has been used in interpreting angular broadening data (see, for instance, Newkirk 1967) and observed with small-scale intensity scintillations (Houminer and Hewish 1974) and large-scale spacecraft measurements (Sullivan, Belcher, and Lazarus 1975). Furthermore, we will use the radial profile of electron density given by Saito (1970). Within 5 $R_\odot$ Saito's model is almost identical to that of Newkirk (1967), and both models represent a widely accepted set of observed coronal densities. Then, since bandwidth B is proportional to $\sigma_{ne}{}^{6/5}v$ (Paper I), a wind velocity profile can be deduced from Figure 4, and the result which is anchored to the velocity measurement at 1.7 $R_\odot$ is shown as a solid line in Figure 8. The important aspect of the coronal density profile in obtaining this result is its shape. Wilson (1976) has shown that the shape given by the Newkirk model, and therefore the Saito model, agrees very well within 5–6 $R_\odot$ with the recent *Skylab* photographs taken by the HAO coronagraph even in streamers. Because the photometric observations are more reliable closer to the Sun, we feel that the deduced wind profile is likewise. For the sake of comparison we have included the radar backscattering measurement made by James (1968) at 38 MHz and the two-station intensity scintillation results obtained by Ekers and Little (1971) at 6.6, 6.8, and 12 $R_\odot$. As can be seen, the combined results in Figure 8 appear to form a consistent wind profile in the acceleration region of the Sun. Moreover, this profile is in reasonable agreement with existing theoretical solar wind models (Hartle and Barnes 1970; Wolff, Brandt, and Southwick 1971; Hundhausen 1972). In the future, extensive and more reliable velocity measurements using two-station observations of phase scintillations (Woo 1977) and the mutual coherence function (Paper

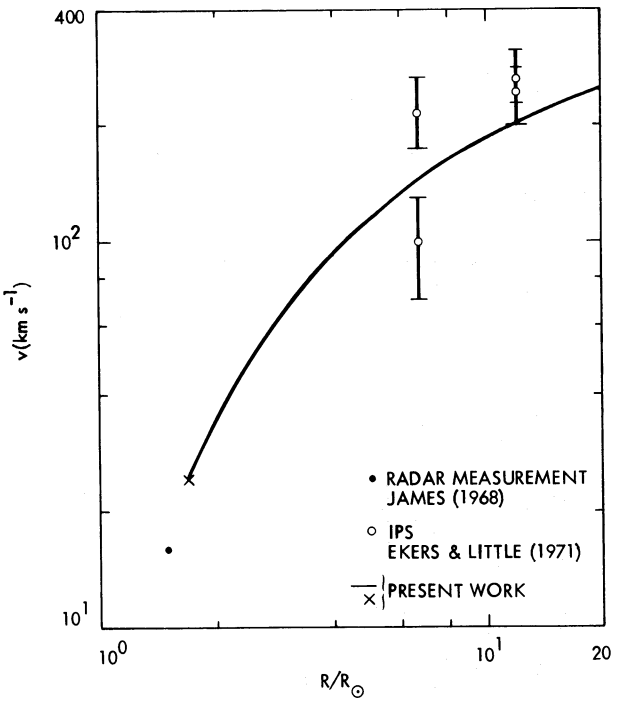

FIG. 8.—Solar wind profile. The measurement at 1.7 $R_\odot$ is obtained from *Helios I* angular and spectral broadening observations, while the solid line is deduced from the spectral broadening results shown in Fig. 4. For comparison, the radar measurement by James (1968) at 38 MHz and the two-station 2.3 GHz intensity scintillation results of Ekers and Little (1971) are also plotted.

II) as well as intensity scintillations will most certainly add substantially to our knowledge of the wind profile near the Sun.

III. PHASE OR DOPPLER SCINTILLATIONS

For over a decade, intensity scintillations of compact radio sources have been used to extensively study the solar wind (see, for example, Hewish 1972; Jokipii 1973; Coles, Rickett, and Rumsey 1974; Lotova 1975). Phase scintillations can be used in much the same way, and in addition they offer several important advantages. The advantages of phase scintillations and their relationship to intensity scintillations for probing the solar wind have been discussed in detail in the literature (Cronyn 1972*a*; Woo 1975; Woo *et al.* 1976; Woo 1977). The realization of the full potential of phase scintillations requires spacecraft signals, because it is only with coherent signals that such measurements can be carried out at a single observing antenna. In contrast, natural radio sources require VLBI observations and these provide information on scale sizes limited to the baseline distance (Cronyn 1972*a*; Mutel 1975).

One problem with spacecraft phase scintillations is that the phase measurements include in addition to the scintillations the effect of the relative motion between the spacecraft and the receiving antenna, and this must be removed before an analysis of the scintillations can begin. Callahan (1975) has used a group-phase velocity technique called Differenced Range versus Integrated Doppler (DRVID) to study the phase scintillations of *Mariners 6*, *7*, and *9*. In DRVID, measurements of range or time-delay are combined with those of phase or Doppler, so that the spacecraft trajectory effect, which is common to both, is eliminated. However, because of the lower resolution of the ranging data, the DRVID technique is limited to probing close to the Sun and to studying slow fluctuations (closest approach distance $R \lesssim 40\ R_\odot$ and fluctuation frequency $f \lesssim 10^{-3}$ Hz in the case of *Mariners 6*, *7*, and *9*).

The spacecraft trajectory is also eliminated in a dual-frequency phase differencing technique recently demonstrated by Woo *et al.* (1976) and currently being applied to the extensive *Viking* S/X observations.[1] Because the S/X technique uses the more highly resolved phase measurements, it is preferred to DRVID.

For missions with a single radio frequency (e.g., *Helios 1/2*, *Pioneer 10/11*), phase scintillations can be measured by subtracting from the observed phase the predicted value due to the spacecraft trajectory. The resulting residuals essentially represent the phase scintillations because the errors in predicting the trajectory are generally considerably lower than the phase scintillations. Since the residuals are based on phase measurements, they are also preferred to DRVID. The fact that the phase residuals represent the phase scintillations is important because it means that *all* past and future NASA deep space missions including those without ranging or coherent dual-frequency capabilities can be used for probing the solar wind, and the study of the solar cycle dependence is possible.

Because residuals are used for navigation purposes, the quantity generally computed is Doppler (frequency) rather than phase. Of course, conversion from one to the other is a simple matter. We have studied the Doppler/phase residuals of *Helios 1* for the period 1975 March 20–June 15 and of *Pioneer 10/11* during the period 1975 February 1–June 15. The *Helios 1* trajectory and the corresponding times are shown in Figure 1. Figure 9 shows the projections of *Pioneers 10* and *11* on the plane perpendicular to the Earth-Sun line. The projection of *Helios 1* is just the ecliptic plane. In the case of *Helios 1* the closest approach distance varied between 1.6 and 68 $R_\odot$; for *Pioneer 10*, between 7.1 and 180 $R_\odot$; and for *Pioneer 11*, between 7.3 and 178 $R_\odot$.

The regular navigational data consist of two-way closed-loop (narrow-band) measurements. The two-way mode is used because the measurements can be referenced to a ground-based frequency standard and are therefore more accurate. It should be pointed out that near the Sun when the scintillations are strong one must be cautious in using this type of data, because the spacecraft transponder and the ground

[1] S-band (13 cm)/X-band (3.5 cm).

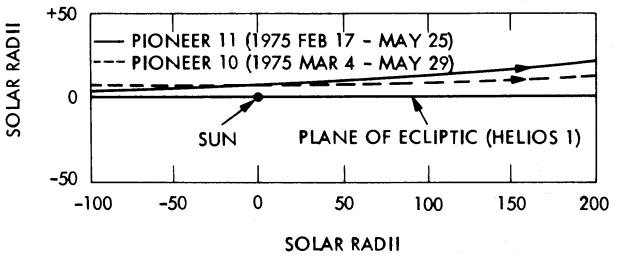

FIG. 9.—The projections of the *Pioneer 10/11* and *Helios 1* orbits on the plane perpendicular to the Earth-Sun line.

receiver are both narrow-band devices and cycle slips will occur. To make matters worse, cycle slips are often difficult to identify as they can be confused with the large phase scintillations. To probe the solar corona near the Sun unambiguously, one must use one-way open-loop (wide-band) measurements such as those described in § II.

The normal sampling rate for the two-way navigational data is 1 per minute. We have spectrum-analyzed the residuals using the same steps discussed in Woo *et al.* (1976). The typical spectrum of the phase residuals shown in Figure 10 is that of *Pioneer 11* observed at a 26 m station at Goldstone on 1975 May 29 when the closest approach distance was 154.2 $R_\odot$ (solar elongation of 45°.8). The span of data analyzed is 6.57 hr long, and the number of adjacent points averaged is 21 (Woo *et al.* 1976). The corresponding 90% confidence limits are indicated, along with a dashed line having a slope of −2.6 and representing an approximation to the measured spectrum. The result in Figure 10 is similar to the *Mariner 10* dual-frequency results (Woo *et al.* 1976). Let us compare them more closely. Since the fluctuation frequency f is much smaller than the Fresnel frequency f_c, we use the following asymptotic result for the frequency spectrum W_ϕ of the phase scintillations given by Woo (1975):

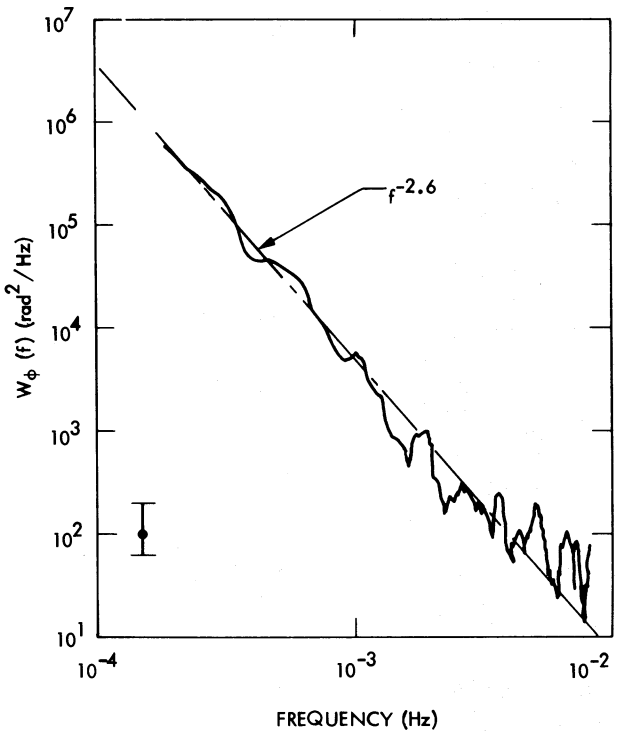

FIG. 10.—Power spectrum of the *Pioneer 11* phase residuals taken on 1975 May 29. The time span is 6.57 hr long. The number of adjacent points averaged is 21. The vertical bar defines the 90% confidence limits. The dashed line corresponds to $f^{-2.6}$.

$$W_\phi(f) = 0.033 c_{n0}^2 k^2 \frac{8\pi^3 a_1 R}{v} \left(\frac{2\pi f}{v}\right)^{1-p} \frac{\Gamma[(p-1)/2]}{\Gamma(p/2)}, \quad (5)$$

where $a_1 = 0.85$ (Woo 1975), $k = 2\pi/\lambda$ is the wavenumber, v is the solar wind velocity transverse to the line-of-sight path at the closest approach point, c_{n0} is the structure constant at the closest approach point, R is the closest approach distance, p is the spectral index of the spatial spectrum of the electron density fluctuations, and Γ is the gamma function. Although equation (5) was derived using Rytov's approximation which is strictly valid only in the case of weak scintillations, Ishimaru (1977) has shown that this result is approximately correct even in the case of strong scintillations. Since equation (5) describes the one-way case, it must be multiplied by 2 for it to be applicable to the two-way mode. For the dual-frequency case, the spectrum $W_{\phi d}$ of the phase-difference scintillations is related to equation (5) by

$$W_{\phi d}(f) = 0.857 W_\phi(f). \quad (6)$$

In the case of *Mariner 10* the closest approach distance $R = 43\ R_\odot$; and at $f = 10^{-3}$ Hz, $W_{\phi d} = 10^5$ rad^2 Hz^{-1}. Multiplying this result by 2 to convert it to a two-way measurement, dividing it by 0.857 to convert it to W_ϕ, and multiplying it by $(43\ R_\odot/154.2\ R_\odot)^{2.6}$ (as we will see later, $W_\phi \propto R^{-2.6}$) to extrapolate to 154.2 $R_\odot$, we obtain 8.43×10^3 rad^2 Hz^{-1}, which agrees fairly well with the *Pioneer 11* result in Figure 10.

Under the Rytov approximation the variance σ_χ^2 of the log-amplitude fluctuations is given by (Paper I)

$$\sigma_\chi^2 \approx k^{7/6} a_1 R (L_1 L_2/L)^{5/6} c_{n0}^2, \quad (7)$$

where L_1, L_2, and L are defined in Figure 7 and $p = 11/3$ (Kolmogorov spectrum) has been assumed. For weak scintillations the scintillation index $m \approx 2\sigma_\chi$ so that

$$m \approx 2k^{7/12} (a_1 R)^{1/2} (L_1 L_2/L)^{5/12} c_{n0}. \quad (8)$$

In analogy to the intensity scintillations we will define a variance σ_ϕ^2 of the phase scintillations

$$\sigma_\phi^2 = \int_{f_1}^{f_2} W_\phi(f) df, \quad (9)$$

where f_1 and f_2 are the chosen limits of the fluctuation

frequency. Similarly, we will define a variance σ_D^2 of the Doppler scintillations

$$\sigma_D^2 = \int_{f_1}^{f_2} W_D(f)df , \tag{10}$$

where W_D is the frequency spectrum of the Doppler scintillations.

Since

$$\text{Doppler (in Hz)} = \frac{1}{2\pi}\frac{\Delta\phi}{\Delta t} , \tag{11}$$

where phase ϕ is in radians, the conversion of phase to Doppler scintillations is equivalent to passing the former through a difference filter whose response is (Jenkins and Watts 1969)

$$\left(\frac{1}{\Delta t}\right)^2 4\sin^2(\pi f_{\text{NORM}}) , \tag{12}$$

where Δt is the sampling interval of the data and the frequency f_{NORM} is normalized to the Nyquist frequency f_N by $f_{\text{NORM}} = f/2f_N$. Combining equations (5), (10), and (12), we obtain for the one-way mode

$$\sigma_D^2 = 0.033 c_{n0}^2 k^2 \frac{8\pi a_1 R}{v}\left(\frac{2\pi}{v}\right)^{1-p}\frac{\Gamma[\frac{1}{2}(p-1)]}{\Gamma(\frac{1}{2}p)} \times \left(\frac{1}{\Delta t}\right)^2 (2f_N)^{2-p} \times \int_{\Delta t/T}^{1} 4 f_{\text{NORM}}{}^{1-p}\sin^2(\pi f_{\text{NORM}})df_{\text{NORM}} , \tag{13}$$

where T is the time duration processed and the effects of aliasing have been included by extending the upper limit of fluctuation frequency f to twice the Nyquist frequency (first aliasing).

We have computed and analyzed σ_D (after removing the constant mean) for the Doppler scintillations of *Helios 1* and *Pioneer 10/11* taken at a sampling frequency of 1 per minute for time spans of 10 min. Assuming the Kolmogorov spectrum ($p = 11/3$), we obtain for the two-way mode

$$\sigma_D = 0.088 c_{n0} k v^{5/6}(a_1 R)^{1/2} . \tag{14}$$

In comparing equation (14) with equation (8), we see that the standard deviation of the Doppler scintillations, contrary to the scintillation index m, depends on velocity v but not on the distances L_1 and L_2. This difference stems merely from the fact that the spectrum W_D extends over an extensive range of f and we are examining just a portion (low frequency) of it. This is significant, because where the variance of the intensity scintillations measures electron density fluctuations, the variance of the phase scintillations is similar to spectral broadening and measures a combination of density fluctuations and velocity. The spectral amplitude at a given fluctuation frequency behaves the same way so that it is incorrect to interpret it as just turbulence (Callahan 1975). One must be particularly careful when using the spectral amplitude to draw conclusions about the radial variation of turbulence near the Sun. We note from equation (14) that since $c_{n0} \propto \sigma_{ne}$, if $\sigma_{ne} \propto n_e$ and $v^{5/6} \sim v$, then σ_D, which is proportional to $\sigma_{ne} v^{5/6}$, is approximately proportional to mass flux.

Typical tracking passes for *Helios* and *Pioneer* were at least 4 hr long. We obtained an average σ_D for each pass by computing and averaging σ_D for running groups of 10 points. As can be seen from Figure 10, there is no problem with SNR even with 26 m stations and large solar elongations because the slowly varying phase scintillations are so strong. We have therefore used the data collected from all 26 and 64 m stations in the Deep Space Net. Since there were typically two or three tracking passes per spacecraft per day, a large data set resulted. The results for σ_D are summarized in Figure 11. For *Pioneers 10* and *11*, measurements closer than 15 $R_\odot$ were excluded since these occurred at high latitudes (see Fig. 9). The results in Figure 11, therefore, represent measurements essentially of the equatorial region. We have also excluded from Figure 11 the *Helios* Doppler measurements within 3.5 $R_\odot$ because they may be ambiguous, as discussed earlier. The few measurements within 10 $R_\odot$ must be regarded with some reservation for the same reason.

For spectral broadening the bandwidth B is (Paper I)

$$B = 0.542(c_{n0}'k)^{6/5}(a_1 R)^{3/5} v , \tag{15}$$

so that $B^{5/6} \propto \sigma_D$. The scale sizes which are responsible for spectral broadening and whose strength is characterized by c_{n0}' are smaller than those responsible for σ_D and characterized by c_{n0} (Paper I). If the small-scale (spectral broadening) and large-scale (Doppler scintillations) electron density fluctuations form a continuous spatial spectrum as appears to be the case (Cronyn 1972*b*; Woo *et al.* 1976), then c_{n0}' would be equal to c_{n0} for a given distance R. Assuming that this is the case, the spectral broadening measurements are related to σ_D by

$$\sigma_D = 0.147 B^{5/6} . \tag{16}$$

Using this result, we have converted the spectral broadening data and included them in Figure 11 and as can be seen the results are quite consistent. It must be emphasized that the purpose of this comparison is to combine the two phenomena in one plot, and is not to show that small-scale and large-scale turbulence form a continuous spectrum even though the results in Figure 11 strongly suggest this. The latter can better be accomplished by other means (Woo *et al.* 1976). It is worth noting that the *Helios* spectral broadening and Doppler scintillations were not observed at the same time since the former were one-way measurements while the latter were two-way. A better comparison would be obtained with simultaneous observations.

The results in Figure 11 demonstrate the remarkable

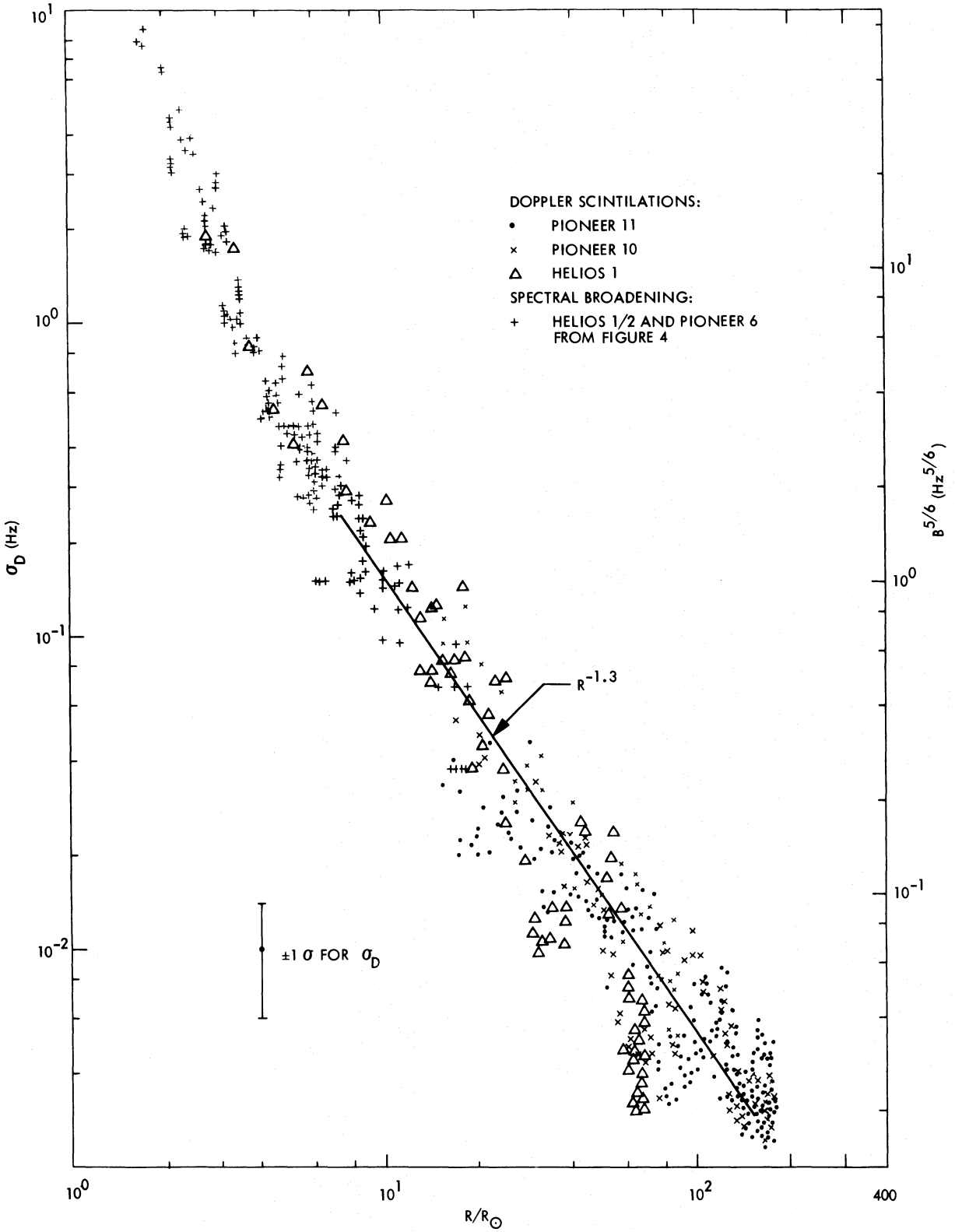

FIG. 11.—Variation of σ_D and $B^{5/6}$ with heliocentric distance

dynamic range of spectral broadening and Doppler scintillations. This dynamic range is possible because neither saturates as do intensity scintillations when they are strong. Far from the Sun the two-way Doppler residuals are limited by the error of the predicted trajectory and the contributions due to the Earth's ionosphere, which are both of the order of a few millihertz. For this reason we have limited the *Pioneer* data to $\sim 180\ R_\odot$. With dual-frequency S/X measurements such as those currently being made with the *Viking* spacecraft, measurements of phase and Doppler scintillations are most likely possible to 1 AU and beyond.

The scatter in the data shown in Figure 11 represents structure such as streams which dominated the solar wind in 1975 (see, for example, Sheely, Harvey, and Feldman 1976). Comparison with direct spacecraft measurements of velocity and density is possible and is currently under way. It is clear from Figure 11 that the structure grows with radial distance and that these measurements provide important information on the evolution of the stream structure. Drawn in Figure 11 is a line representing the radial dependence $R^{-1.3}$ and, as can be seen, it is a fairly good approximation to the data for distances greater than $10\ R_\odot$. Since the spectrum is proportional to the variance, W_ϕ and W_D are both proportional to $R^{-2.6}$. From equation (14) we see that the $R^{-1.3}$ variation corresponds to $\sigma_{ne} v^{5/6} \propto R^{-2}$, so that within the assumption that $\sigma_{ne} \propto n_e$ and $v^{5/6} \sim v$, mass flux is approximately proportional to $R^{-1.8}$, suggesting a solar wind that is slightly converging in the equatorial region between approximately 20 and $180\ R_\odot$, a result that is not unreasonable (Suess *et al.* 1977). Intensity scintillations (Armstrong and Coles 1978; Sime 1976) show that small-scale density fluctuations have an approximate radial dependence of $R^{-2.05}$. If we assume that the small- and large-scale sizes are proportional and use equation (14), we find that a radial dependence of $R^{-1.3}$ for σ_D implies that $v \propto R^{0.3}$. Extending the results shown in Figure 8 to 1 AU according to this variation yields a velocity of 509.8 km s^{-1}, which is comparable to direct spacecraft measurements (private communication with A. Lazarus and J. Sullivan) in 1975.

It is important to point out that the purpose of the above discussion is to show that a rough interpretation of the Doppler scintillations yields results that are consistent with other observations. It is clear, however, that stronger conclusions are possible if coordinated observations of intensity and phase scintillations and group delay are conducted.

IV. CONCLUSIONS AND DISCUSSION

We have presented spectral broadening measurements made closer to the Sun than ever before. When combined with the first observation of angular broadening of a spacecraft signal, we obtain a measurement of the solar wind velocity of 24 km s^{-1} at $1.7\ R_\odot$, an estimate which should be accurate to within a factor of 2–2.5. We have also measured the wind velocity profile in the acceleration region of the solar wind by assuming $\sigma_{ne} \propto n_e$ and using Saito's electron density profile. These results are consistent with other scarce velocity measurements of the acceleration region as well as existing theoretical models of the solar wind.

At $1.7\ R_\odot$ the loss in signal power due to angular broadening using the 64 m antenna is significant. Any increase in transmitted power that is likely to occur in future missions will be small when compared with this loss, and will therefore not be effective in probing closer to the Sun. On the other hand, because the antenna beamwidth is proportional to k^{-1} while angular broadening is proportional to $k^{p/(2-p)}$, increasing the radio frequency will result in closer measurements. We have recently demonstrated this with the *Viking* X-band signal by obtaining measurements closer than $1.5\ R_\odot$.

Predictions for the spacecraft trajectory are accurate enough that closed-loop two-way Doppler or phase residuals essentially represent scintillations. This is an important result because large amounts of such data are available for all past NASA deep space missions and can be retrieved for the purposes of studying the solar cycle variation. The fact that the residuals are the scintillations also means that multiple-station wind velocity observations, recently proposed by Woo (1977), can be conducted even when the spacecraft has only one frequency as in the case of *Helios*. Because Doppler measurements are better resolved than ranging measurements, Doppler residuals are superior to DRVID for probing the solar wind. As a result, we have found that the *Pioneer 10/11* data are useful as far out as $180\ R_\odot$. The Doppler scintillations, which are shown to be proportional to $\sigma_{ne} v^{5/6}$, have a radial dependence of $R^{-1.3}$ and, within the assumptions that $\sigma_{ne} \propto n_e$ and $v^{5/6} \sim v$, suggest that the solar wind is slightly converging in the equatorial region between approximately 20 and $180\ R_\odot$.

Near the Sun where the scattering is strong, the only reliable and unambiguous measurements are those performed in the one-way mode using an open-loop receiver, such as the *Helios* spectral broadening observations. In the two-way mode, cycle slips may occur in the transponder; and if a closed-loop receiver is used, cycle slips may occur there too. For the purposes of studying phase scintillations or changes in total electron content, if the choice is between one-way and two-way, it should be one-way; if the choice is between one-way open loop and one-way closed loop, it should be the former; and if the choice is between DRVID and Doppler residuals, it should be the Doppler residuals.

It is clear that spacecraft radio scattering measurements have emerged as an important tool for probing the solar wind. Observations can now be made closer to the Sun and over a wider range of scale sizes and heliocentric distances than have ever been possible before. The dynamic range of spectral broadening and phase scintillations is large because neither saturates. As a result, these measurements are sensitive

and useful for studying not only the radial, latitudinal, and solar cycle dependence of the solar wind, but also temporal variations such as stream structure, transients, and events. Further systematic observations will surely improve our understanding of the dynamics and acceleration of the solar wind, the origin and evolution of high-speed streams, and their relationship to coronal holes near the Sun.

It is a pleasure to acknowledge and thank G. Levy, C. Stelzried, K. Heftman, A. Beers, A. Bouck, and the *Helios* Project Office for support throughout these experiments, B. Seidel and K. Wallace for instrumentation, W. Hudson and his group for diligently collecting the spectral broadening data, N. Feagans and W. Kirhofer for retrieving the *Pioneer* Doppler residuals, R. Emerson and J. Wackley for generating the predicts for the programmed local oscillator, and F. C. Yang for assistance in data processing. I am especially indebted to R. M. Goldstein for letting me use his equipment and analysis programs and for giving freely of his time and advice in conducting the experiment, and to J. W. Armstrong with whom I had many useful and stimulating discussions. In carrying out this research, I have benefited from my participation in one of the *Skylab* Solar Workshops on Coronal Holes. The Workshops are sponsored by NASA and NSF and managed by the High Altitude Observatory. This paper presents the results of one phase of research carried out at the Jet Propulsion Laboratory, California Institute of Technology, under contract NAS7-100, sponsored by the National Aeronautics and Space Administration.

REFERENCES

Armstrong, J. W., and Coles, W. A. 1978, *Ap. J.*, in press.
Bathker, D. A. 1973, AGARD Conference Proceedings, No. 139, 29–1.
Blesing, R. G., and Dennison, P. A. 1972, *Proc. Astr. Soc. Australia*, **2**, 84.
Callahan, P. S. 1975, *Ap. J.*, **199**, 227.
Cohen, M. H., and Gunderman, E. J. 1969, *Ap. J.*, **155**, 645.
Coles, W. A., Rickett, B. J., and Rumsey, V. H. 1974, *The Solar Wind, III* (Los Angeles: University of California), p. 351.
Cronyn, W. M. 1972*a*, *Ap. J.*, **174**, 181.
———. 1972*b*, *Ap. J.* (*Letters*), **171**, L101.
Dennison, P. A., and Blesing, R. G. 1972, *Proc. Astr. Soc. Australia*, **2**, 86.
Ekers, R. D., and Little, L. T. 1971, *Astr. Ap.*, **10**, 310.
Erickson, W. C. 1964, *Ap. J.*, **139**, 1290.
Goldstein, R. M. 1969, *Science*, **166**, 598.
Hartle, R. E., and Barnes, A. 1970, *J. Geophys. Res.*, **75**, 6915.
Hewish, A. 1958, *M.N.R.A.S.*, **118**, 534.
———. 1972, *The Asilomar Conference on the Solar Wind*, p. 477.
Hewish, A., and Symonds, M. D. 1969, *Planet. Space Sci.*, **17**, 313.
Houminer, Z., and Hewish, A. 1974, *Planet. Space Sci.*, **22**, 1041.
Hundhausen, A. 1972, *Solar Wind and Coronal Expansion* (New York: Springer-Verlag).
Ishimaru, A. 1977, *Appl. Optics*, in press.
James, J. C. 1968, in *Radar Astronomy*, ed. J. V. Evans and T. Hagfors (New York: McGraw-Hill), p. 323.
Jenkins, G. M., and Watts, D. G. 1968, *Spectral Analysis and Its Applications* (San Francisco: Holden-Day), p. 296.
Jokipii, J. R. 1973, *Ann. Rev. Astr. Ap.*, **11**, 1.
Jokipii, J. R., and Lee, L. C. 1972, *Ap. J.*, **172**, 729.
———. 1973, *Ap. J.*, **182**, 317.
Kliore, A., Cain, D. L., and Hamilton, T. W. 1964, Jet Propulsion Laboratory Tech. Rept. No. 32–674.
Lotova, N. A. 1975, *Soviet Phys. Uspekhi*, **18**, 292.
Mutel, R. L. 1975, Ph.D. thesis, University of Colorado.
Newkirk, G. 1967, *Ann. Rev. Astr. Ap.*, **5**, 213.
Okoye, S. E., and Hewish, A. 1967, *M.N.R.A.S.*, **137**, 287.
Rao, A. P., Bhandari, S. M., and Ananthakrishnan, S. 1974, *Australian J. Phys.*, **27**, 105.
Saito, K. 1970, *Ann. Tokyo Astr. Obs.*, **12**, 53.
Sheeley, N. R., Harvey, J. W., and Feldman, W. C. 1976, *Solar Phys.*, **49**, 271.
Sime, D. G. 1976, Ph.D. thesis, University of California San Diego.
Slee, O. B. 1966, *Planet. Space Sci.*, **14**, 255.
Suess, S. T., Richter, A. K., Winge, C. R., and Nerney, S. F. 1977, *Ap. J.*, **217**, 296.
Sullivan, J. D., Belcher, J. W., Lazarus, A. J. 1975, *EOS Trans. AG4*, **56**, 440.
Vitkevich, V. V., and Vlasov, V. I. 1972, *Soviet Astr.—AJ*, **16**, 480.
Waldmeier, M. 1977, *Nature*, **265**, 611.
Ward, B. D. 1975, Ph.D. thesis, University of Adelaide.
Wilson, D. 1976, Ph.D. thesis, University of Colorado.
Watanabe, T., Shibasaki, K., and Kakinuma, T. 1971, *J. Geophys. Res.*, **79**, 3841.
Wolff, C. L., Brandt, J. C., and Southwick, R. G. 1971, *Ap. J.*, **165**, 181.
Woo, R. 1975, *Ap. J.*, **201**, 238.
———. 1977, *Nature*, **266**, 514.
Woo, R., Yang, F. C., and Ishimaru, A. 1976, *Ap. J.*, **210**, 593 (Paper I).
———. 1977, *Ap. J.*, **218**, 557 (Paper II).
Woo, R., Yang, F. C., Yip, K. W., and Kendall, W. B. 1976, *Ap. J.*, **210**, 568.

RICHARD WOO: Jet Propulsion Laboratory 238/737, 4800 Oak Grove Drive, Pasadena, CA 91103